Eur. Phys. J. B **22**, 485–495 (2001)

THE EUROPEAN PHYSICAL JOURNAL B

EDP Sciences

Growth velocity and the topography of Ni-Zn binary alloy electrodeposits

M. Hiane and J. Ebothé[a]

Unité de Thermique et d'Analyse Physique - LMET, UPRES EA n° 2061, UFR Sciences Exactes, Université de Reims, BP 138, 21 rue Clément Ader, 51685 Reims Cedex 02, France

Received 16 August 2000 and Received in final form 20 June 2001

Abstract. We show that the electrodeposition of Ni-Zn alloys at the lowest growth velocities, $v < 0.5$ μm/s, exclusively proceeds from an abnormal co-deposition phenomenon. The growth process in this v region greatly depends on the initial $[Co^{2+}]$ concentration of the film deposition bath. A theoretical approach of this process including the role of the saturation surface roughness of the alloy, σ_{sat}, leads to an estimation of the transport properties of the ad-atoms involved during the deposit formation. Their surface diffusion coefficient varying between 1.76×10^{-10} and 2.40×10^{-8} cm^{-2}/s exhibits a minimal value, $D_s = 2.10 \times 10^{-10}$ cm^{-2}/s located between $v = 0.17$ and 0.35 μm/s. The spatial scaling analysis of the local roughness, σ, examined according to the power-law $\sigma \approx L^{\alpha}$ reveals that the resulting roughness exponents concurs with the Kardar-Parisi-Zhang dynamics including the restricted surface diffusion. Two main v regions leads to different fractal textural features of the alloy film surface. Below 0.10 μm/s, the roughness exponent obtained is $\alpha \approx 0.6$, depicting a limited ad-atom mobility. Over $v = 0.30$ μm/s, this exponent stabilises at $\alpha \approx 0.82$, indicating an increase of the surface diffusion.

PACS. 81.15.Aa Theory and models of film growth – 68.35.Ct Interface structure and roughness – 61.82.Bg Metals and alloys

1 Introduction

Alloying of zinc by iron group elements (Ni or Co) has been the subject of extensive research mainly directed towards two different fields: the corrosion resistance and the catalytic activity. From the first viewpoint, many authors reported on the important role of the alloy composition, indicating that the optimal corrosion resistance is reached for the alloy nickel content between 12 and 13% [1,2]. This compositional aspect also accounts for the performance of the Raney nickel coating commonly recognised as an excellent electrocatalyst whose activity results from the leaching of Zn element in the Ni-Zn alloy [3,4]. In both fields, the searched-for property is determined by the material active surface. The corrosion protection needs a low surface area while the catalytic role necessitates the highest one. Evidently, the surface quality proceeds from how the material growth process has been addressed, that determines its final microstructure. In this framework, the relationship between the preparation conditions, the growth and the microstructure of Ni-Zn and Co-Zn alloy electrodeposits has been widely investigated from the images of both, the scanning (SEM) and the transmission (TEM) electron microscopies. Fratresi *et al.* [5,6] report on the effect of the deposition bath composition. Miranda *et al.* [7] reveal a variety of surface patterns, extending these investigations on the role of some other parameters such as pH, applied potential, current density, bath concentration, deposition temperature and so on. Some authors focus on the influence of the phenolic derivatives [8] and the boric acid [9] reagents. By and large, this classical approach remains descriptive and it becomes unsatisfactory when an attempt is made to correlate the surface microstructure with another physical or chemical property of the material. The use of quantitative parameters is needed in this case, that allows the modelling of this correlation and leads to a more easy comparison of experimental results. For that reason, topographical parameters can characterise the material surface microstructure.

The modern industrial trend of reducing the sample surface and thickness leads to furthermore consider the surface effect on the material properties, that is by now fully recognised but not clearly explained [10,11]. *A priori*, the understanding of this effect requires an accurate control of the surface growth at the mesoscopic scales, keeping in mind that the material physical, chemical and mechanical properties are initiated at these low dimensions. High resolution methods are appropriate in this case, the technology of the scanning probe microscopy (SPM) being thus well adapted. So far, this research orientation is mainly devoted to thin films generated by non-equilibrium processes. In this frame, simulation and modelling studies aim to predict a surface pattern from a particular growth scheme are reported. Family *et al.* [12,13]

[a] e-mail: jean.ebothe@univ-reims.fr

provide a review of the different models linked to the film deposition by the physical methods that engender a local process whilst Sander *et al.* [14–16] report on those of the formation in wet media depicting a non local process. In practice, this separation may be less systematic, particularly when electrodeposition technique is concerned. To determine whether a film growth process belongs to one of the two categories, it is necessary to examine the material surface through the scaling theory as presented by Meakin [17]. This method is based on the behaviour of two quantitative statistical parameters *i.e.* the root-mean-square surface roughness σ and the lateral correlation length L_c, which are both characteristics of its topography. σ represents the measure of the vertical fluctuation of the surface irregularities whilst L_c corresponds to the lateral coarsening. Their behaviour is followed with respect to the scan length L of the film surface area for the static or spatial study, the film thickness or the deposition duration being the variable for the dynamic aspect. The results obtained from real surfaces are compared to those of the models in order to assess their reciprocal compatibility.

It should be pointed out that the reported topographical models and experimental results mostly concern the surface growth of mono-atomic materials whose thermodynamic, physical and chemical characteristics are well known. Those of the alloys and composite materials as Ni-Zn are expected to vary with their chemical composition. Some interesting topographical evolutions recently reported on such mixed materials evidence the dependence of σ on some particular deposition parameters [18]. This appears the only way to find out adequate metal surface patterns for various applications avoiding foreign additives. Similarly, we here consider the effect of the deposition velocity v on the surface growth and the topography of nickel-zinc alloy electrodeposits. The study is focused on the lowest velocities, $v < 0.5$ μm/s, whose resulting samples are commonly considered as having no real practical application [1,2]. Conversely, they present a fundamental interest since they lead to the smoothest deposits whose surface analysis can be executed with the high resolution methods. The aim of the present work is to show that v value, taken in the investigated region, affects the material growth mode whose resulting surface pattern can also be explored. We propose for the outline, an experimental Section 3 including the composition, the morphology and the topography aspects. A brief theoretical approach of the surface growth as used for the interpretation of the results is proposed in Section 4. A discussion on the material formation and the universality class of the interface growth involved is presented in Section 5.

2 Experiment

One deals in the present work with 2 μm-thick binary alloy Ni-Zn electrodeposits prepared from a three-electrode cell system made of: a stationary copper working electrode of 0.5 cm^2 area (purity 99.99%) mechanically polished on successive rotating disks; a platinium sheet counter electrode of the same area facing the first one 2.5 cm away and a saturated calomel electrode (SCE) as reference for the potential measurements. The electrolyte is a mixed bath made of FLUKA 0.9 M $NiSO_4.6\,H_2O$ and 0.1 M $ZnSO_4.7\,H_2O$ solutions whose pH value is maintained at 3.5 by a small addition of sulfuric acid. During the alloy formation, all the cell system is kept at a constant temperature $T = 323$ K under a 300 t/min magnetic stirring. The electrodeposition is performed by means of a Radiometer PGP 201 galvanostat using the current constant mode that is more suitable for the control of the mass deposition and the study of the alloy composition. The film deposition duration is adjusted to the applied current density J to keep constant the resulting film thickness. v is deduced from J according to the Faraday law:

$$v \approx \frac{MR}{Fz\rho}J, \tag{1}$$

assuming that the deposition efficiency is $R = 1$ with F, the Faraday number; $z = 2$, the common molar charge of the nickel and zinc ion species. Owing to the fact that the binary alloy consists of two molar weight elements, the value M retained here is an average of those related to each of them. The same procedure is applied for the evaluation of the alloy density ρ.

The film composition is determined by X-ray energy dispersive spectroscopy using an EDAX 9100 analyser. The percentage of each one of the two alloy elements is calculated according to the Brenner's relationship here expressed for the case of nickel element [19], such as:

$$Ni(\%) = \frac{\text{mass Ni}}{\text{mass(Ni + Zn)}} \times 100. \tag{2}$$

The spatial scaling analysis of the sample surface is investigated by atomic force microscopy (AFM). A Digital Instruments Nanoscope II set up used for that purpose operates in a constant force contact mode with a cantilever made of a Si_3N_4 tip of approximately 50 nm apex radius whose spring coefficient is 0.06 Nm^{-1}. The topographical measurements is performed in ambient atmosphere, the images being digitised into 400×400 pixels with a scanning frequency of about 1 Hz. The σ retained is an average value resulting from several samples strictly deposited under the same conditions. The error bar is estimated less than 10%. Notes that after polishing, therefore before the electrodeposition is performed, the bare copper substrate bears a σ value close to 10 nm. This value is so largely lower than the film thickness (2 μm) that it can be considered as having no effect on the surface topography of the investigated Ni-Zn deposits.

3 Results

In the electrodeposition of a mono-atomic material, the influence of v on the deposit properties can be safely investigated keeping constant all the other deposition parameters. Regarding alloy electrodeposits, the variation of v prompts a co-deposition phenomenon that affects all

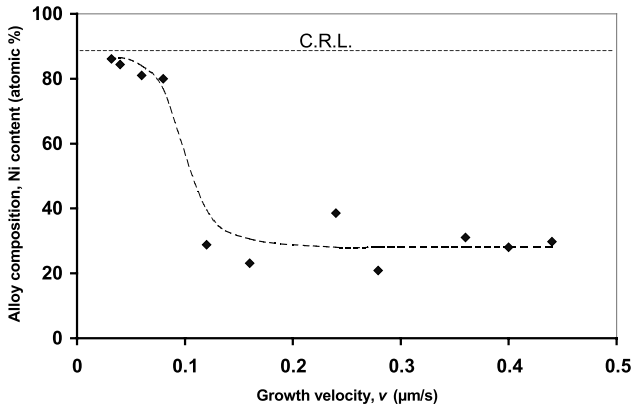

Fig. 1. Evolution of the Ni-Zn alloy composition with respect to the growth velocity.

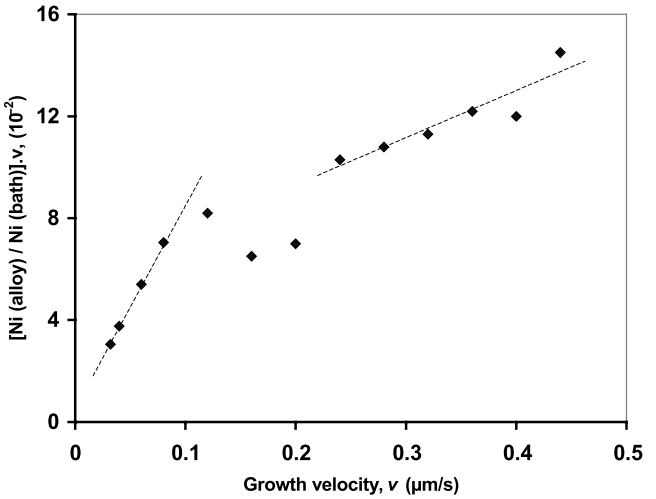

Fig. 2. Characteristics of the co-deposition phenomenon in the formation of the Ni-Zn alloy electrodeposits.

the material microstructure aspects [18]. For that reason, we first analyse in the present section the evolution of the alloy composition before considering the morphology and the surface growth aspects.

3.1 Co-deposition phenomenon and the Ni-Zn alloy composition

Figure 1 shows that the nickel content of the Ni-Zn alloy varies with the growth velocity. One notes that for $v < 10$ nm/s, the percentage of this element remains located between 80 and 90% while a striking decrease towards a mean value of approximately 30% is immediately obtained over this v value. This behaviour presumably denotes the existence of two compositional regimes and raises the problem of normality in the co-deposition process. The reports on the electrodeposition of alloys made of Zn and the iron group elements reveal that low concentrations of the more noble species in the bath leads to an abrupt transition from normal to abnormal co-deposition phenomenon with the increasing of the growth velocity [5–7]. The normal process is observed at reduced v values, the abnormal one appearing at the highest velocities. This deviation occurs at a specific transition velocity v_{T} and the related percentage decrease is always crossed by the compositional reference line (CRL) that corresponds to the point of the $(X\%) = f(v)$ curve where the content of the more noble metal in the deposit is equal to the one in the bath. The results observed from the $[\mathrm{Ni}^{2+}/\mathrm{Zn}^{2+}]$ and $[\mathrm{Co}^{2+}/\mathrm{Zn}^{2+}]$ electrolytes, irrespective of the media pH values, broadly exhibit a related percentage decrease of approximately 90 units. Fratesi *et al.* [6] show that this compositional transition is greatly affected by the deposition temperature. It is easily obtained in ambient temperature and at $T = 323$ K for instance this transition occurs within the normal co-deposition zone for the noble metal content in the bath less than that of Zn. The results of Figure 1 depicts a similar behaviour, the decreasing movement being quite located in the abnormal co-deposition zone, below the CRL limit. It can be pointed out that the electrodeposition is here performed at relatively high temperature as above but the Ni content in the bath (90%) is largely higher than that of Zn.

Table 1. Characteristics of the abnormal co-deposition phenomenon of the Ni-Zn alloy from the decreasing regime of $\mathrm{Ni_{al}}$ with respect to $\mathrm{Ni_{sol}}$ as shown in Figure 2.

Linear zones	k_1	k_2
$v < 0.10$ μm/s	0.10	20.7
$v > 0.20$ μm/s	2.21	2.94
From Feloni *et al.* [6]	0.30	1.37

This abnormal co-deposition is examined following the behaviour of the ratio between the nickel content of the alloy ($\mathrm{Ni_{al}}$) under the one in the plating bath ($\mathrm{Ni_{sol}}$) against v. The profile of the curve in Figure 2 exhibits two quasi-linear zones precisely located below 0.10 μm/s and over 0.20 μm/s. In this study, the linearity denotes an hyperbolic deviation of $\mathrm{Ni_{al}}$ from $\mathrm{Ni_{sol}}$ with the increase of v, according to equation:

$$\frac{\mathrm{Ni_{al}}}{\mathrm{Ni_{sol}}} = \frac{k_1}{v} + k_2. \tag{3}$$

This behaviour concurs with the empirical curve profile previously reported in the case of the deposition baths for which the nickel content is less than 40% [5,6]. However, only one linearity is observed in that case, the experiment being exclusively executed at higher v values. The results in Table 1 show that the decrease of $\mathrm{Ni_{al}}$ in the two v regions corresponds to different regimes, each one of them being characterised by specific k_1 and k_2 coefficients. Individually, their values differ from those of the single linear feature of the curve proposed by Fratesi *et al.* [5,6].

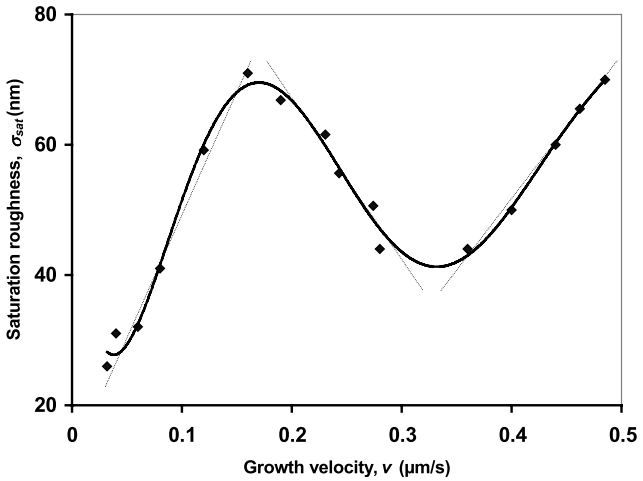

Fig. 3. Behaviour of the saturation surface roughness measured at $L = 15$ μm for the Ni-Zn alloy electrodeposits with respect to the growth velocity.

3.2 Saturation surface roughness and morphology of the Ni-Zn alloy films

We here measure σ in a relative large scan length region. For that purpose, the smallest L values provide only a local roughness whose evolution with the increase of L serves for the scaling analysis, as presented in Section 3.3. The largest L values promptly lead to the stationary or saturation roughness of the surface, $\sigma_{\rm sat}$, that represents the expanded topography of the sample surface intimately associated with its deposition conditions. We point out that $\sigma_{\rm sat}$ is already reached here for $L = 15$ μm in every case and therefore it serves for the study of the growth velocity effect. Figure 3 shows that the plot of $\sigma_{\rm sat}$ *versus* v linearly increases till approximately 0.16 μm/s that is followed by a parabolic-like profile whose minimum position practically corresponds to the curve point (0.32; 42). This behaviour goes together with a morphological evolution of the film surface clearly depicted in the AFM 3D-images of Figure 4. One observes that low velocities, represented here by $v = 0.04$ μm/s give rise in Figure 4a to a high density of needle-like small grains whose growth orientation is normal to the deposition substrate. The increase of v till 0.16 μm/s engenders a sensitive increase of the grain size along with a tremendous lowering of the grain density portrayed in Figure 4b. Nevertheless these grains broadly have the same shape than the last ones, keeping also the same growth orientation. It can be easily inferred that the linear increase of $\sigma_{\rm sat} = f(v)$ curve as obtained in Figure 3 till 0.16 μm/s is caused by the regular increase of the structure size. The surface microstructure of Figure 4d obtained at the highest velocities *e.g.* $v = 0.44$ μm/s is characterised by the top-rounded large grains that have a more longitudinal shape, their inter-granular zones being deeper than in the preceding cases. Between the last two configurations there is an intermediate morphology of Figure 4c that corresponds to $v = 0.28$ μm/s. The growth orientation of the grains is here less evident, the structure size being markedly reduced in comparison to those obtained at the lower and higher v values.

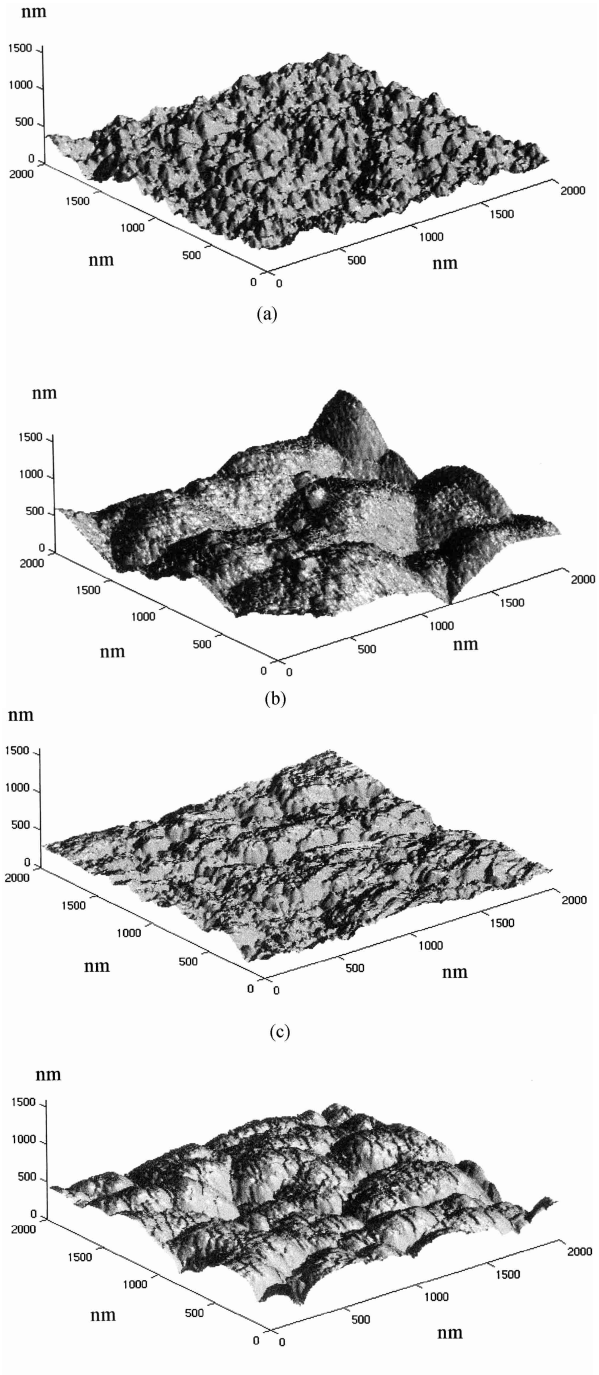

Fig. 4. AFM 3D surface images of the Ni-Zn alloy electrodeposits obtained at different growth velocities: (a) $v = 0.04$ μm/s; (b) $v = 0.16$ μm/s; (c) $v = 0.28$ μm/s; (d) $v = 0.44$ μm/s.

3.3 Scaling analysis of the Ni-Zn alloy film surface roughness

The method applied is based on the theoretically predicted behaviour of the space-time interface width (the mean surface height fluctuation), represented here by the surface roughness $\sigma(L, t)$ [17,18] scales as

$$\sigma(L, t) \propto L^{\alpha}, \quad \text{for } L \ll L_{\rm c}. \tag{4}$$

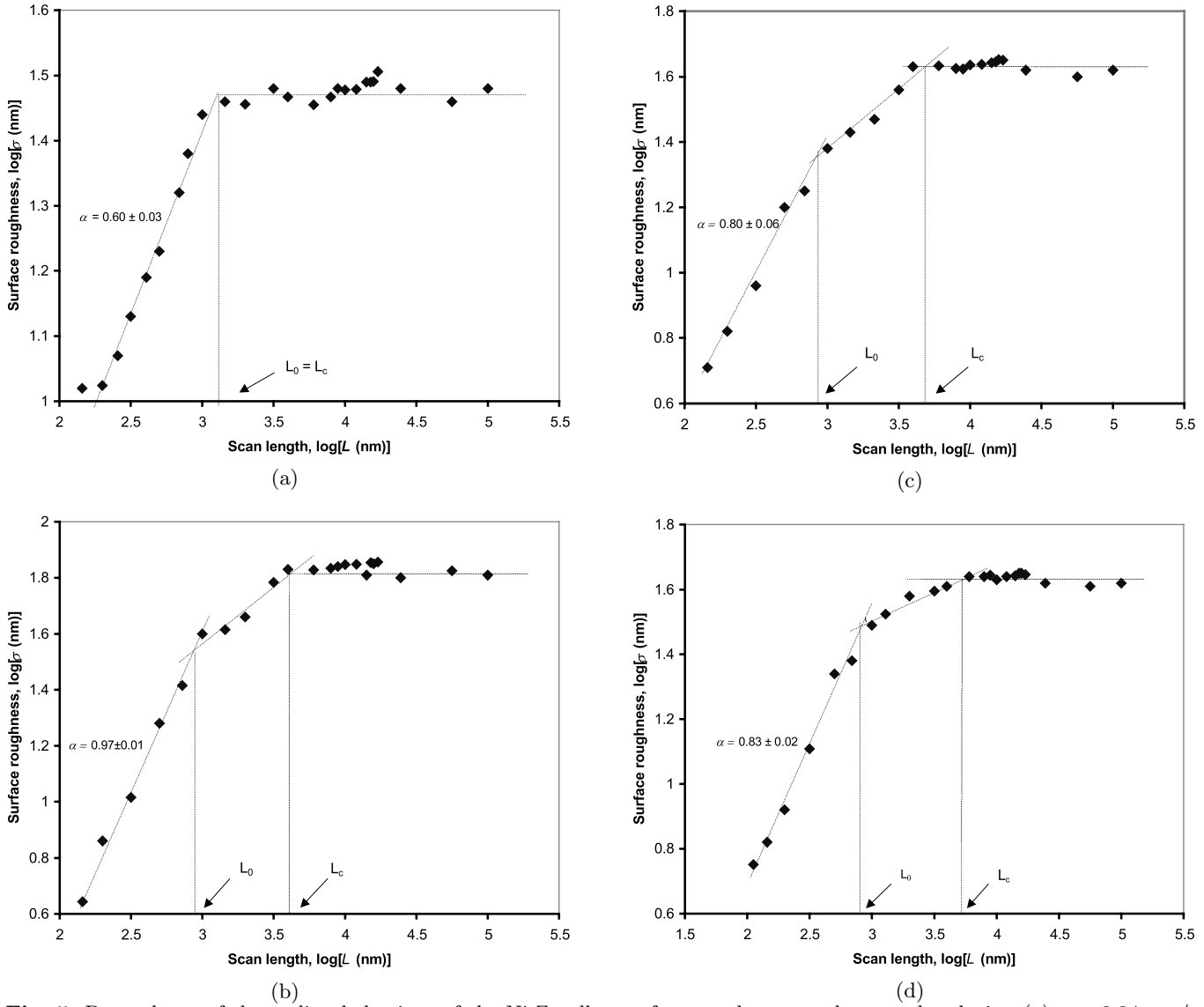

Fig. 5. Dependence of the scaling behaviour of the Ni-Zn alloy surface roughness on the growth velocity. (a) $v = 0.04$ μm/s; (b) $v = 0.16$ μm/s; (c) $v = 0.28$ μm/s; (d) $v = 0.36$ μm/s.

The plotting of the $\log \sigma = f(\log L)$ curves for a constant t value aims to give a picture of the surface growth from the study of the curve region located below the saturation regime. A linear behaviour in this L region corresponds a slope α known as the roughness or Hurst exponent that is one of the main topographical parameter used to determine the universality class of the interface growth [12–16].

The dependence of the curve profile on the growth velocity appears to be typical of a particular range of v values. One observes for $v < 0.10$ μm/s that the scaling step always exhibits a single sloped linear part as shown in Figure 5a for $v = 0.040$ μm/s. We point out that one deals with the Ni richest phases of the alloy (Ni content $>$ 80%) whose structure and composition are approximately those of the pure nickel electrodeposit. Similar results are reported in reference [18] with the electrodeposits of the different iron group elements (Co, Ni and Fe) although the experiment is executed in this case at higher v values. This particular behaviour seems to be only specific of this material group since it is not observed in Figure 5c with the Zn-rich alloy sample. A sensitive decrease of the Ni content in the alloy leads to another specific common feature characterised by a double-linear curve profile preceding the saturation zone. As depicted in Figures 5b, c and d, the two linear parts intersect at a crossover length L_0 always deviated from the lateral correlation length L_c defined as the particular L value of the saturation onset. This deviation, also observed with the Co-based alloys [18], implies some microstructure change induced by the growth velocity. It has been considered as a non trivial scaling by Family [20] caused by surface diffusion effects. The difference $\Delta L = L_c - L_0$ depicting this deviation increases with the increasing of v value as it appears in Table 2.

Table 2. Evolution of the crossover (L_0) and the lateral correlation (L_c) lengths *versus* v of the Ni-Zn alloy surfaces according to the results of Figure 5.

Growth velocity v (μm/s)	L_0 (μm)	L_c (μm)	ΔL (μm)	L_c/L_0
0.04	1.12	1.12	0.00	1.00
0.16	1.12	5.62	4.50	5.01
0.28	0.80	3.95	3.15	4.93
0.36	0.73	3.96	3.23	5.42

Table 3. Behaviour of the Hurst exponent related to the Ni-Zn alloy surfaces with respect to the growth velocity.

Sample designation	Ni content (%)	Growth velocity v (μm/s)	Hurst exponent
A2	84	0.04	$\alpha = 0.60 \pm 0.03$
A8	25	0.12	$\alpha = 0.82 \pm 0.02$
A9	23	0.16	$\alpha = 0.97 \pm 0.01$
A12	17	0.28	$\alpha = 0.80 \pm 0.06$
A14	31	0.36	$\alpha = 0.83 \pm 0.02$
A15	30	0.40	$\alpha = 0.82 \pm 0.03$
A16	29	0.44	$\alpha = 0.81 \pm 0.05$

The Hurst exponents deduced from the scaling curves reveals in Table 3 that the Ni-Zn alloy prepared at $v = 0.04$ μm/s leads to $\alpha = 0.60$ which results from a single linear sloped portion of the curve as obtained in Figure 5a. Nearly the same α is obtained for $v < 0.1$ μm/s, that is also the value reported for pure Ni electrodeposits prepared at a higher velocity ($v = 5.47$ μm/s) [18]. The splitting of the curve linearity in Figure 5 for $v > 0.1$ μm/s suggests some relationship with the behaviour of σ_{sat} *versus* v to be underlined. Actually, the increase of σ from 0.60 to 0.97 in Table 3 seems to accompany the one of σ_{sat} in Figure 3 below $v = 0.16$ μm/s. However, if α decreases till approximately 0.81 over this v value, a minimum at the position (0.32; 41) is observed in the $\sigma_{sat} = f(v)$ curve for the same v region. We point out that the narrow L regions related to the second linear behaviour of the curves in Figure 5 are irrelevant for the determination of a second roughness exponent. This curve region is thereby considered as a simple crossover zone between the first scaling and the saturation regimes. The results as obtained imply some modifications in the material formation process that can be elucidated in the light of a theoretical analysis.

4 Theoretical background

The interpretation of the results as obtained requires an adequate description of the morphological evolution of the film surface during the film formation including the kinetics of roughening. This is proposed by Vazquez *et al.* [21] as regards electrodeposits. This approach is an extend of the Ostwal ripening model based on the formation of adatoms and their mobility on the substrate that is adapted to the specificity of the electrodeposition method [22,23]. The growth process is here broadly summarised into three steps: 1) the formation of the nucleation sites at the early stage of the crystallization; 2) the development of the adatoms or particles becoming aged structures or grains till their critical concentration gradient is reached; 3) the coalescing of these grains prompted by the surface diffusion of the ad-atoms from the sites of higher to the sites of lower chemical potentials. This time dependent process can be evaluated from the size increase of the coalescing particle radius r which obeys the law [24]:

$$\frac{\partial(r^4)}{\partial t} = \frac{2\gamma\, a^4 D_s}{\varepsilon_T}, \tag{5}$$

where a is the lattice parameter; D_s, the surface diffusion coefficient; γ and ε_T, respectively the interface and the thermal energies. The grain size can be evaluated by the integration of equation (5) from zero to t as:

$$r^4 - r_0^4 = \frac{2\gamma\, a^4 D_s t}{\varepsilon_T} \tag{6}$$

with r_0 the initial particle radius and r, the average grain size at any time t. If one assumes that r_0 is of the atomic size order, it can be neglected compared to r from a certain range of t value. In this case, equation (6) is simplified into:

$$r^4 \approx \frac{2\gamma\, a^4 D_s t}{\varepsilon_T}\,. \tag{7}$$

This equation denotes the possibility to determine D_s from the measurement of r with t. It is shown elsewhere that r is directly linked to the roughness factor of the electrodeposit [24]. This factor can be expressed in terms of three dimensional root-mean-square surface roughness, σ, obtained from SPM measurements. We notify that the relationship between r and various roughness parameters of a surface has been investigated by Carneiro *et al.* [25] who reported on the direct proportionality between r and σ. Therefore, the determination of D_s as proposed becomes possible following the behaviour of σ with t.

If the surface morphology is here modelled in a close packed array of columns as proposed by Alonso *et al.* [24], the instantaneous relationship between σ and r can be expressed as:

$$\sigma = \frac{\pi\, h}{2\, r}, \tag{8}$$

where h stands for the average columnar height whose average radius r fulfilled the condition $h \ll r$. If one assumes that the ageing process leads to a highly faster increase of r compared to that of $h(\delta h/\delta t \ll \delta r/\delta t)$, one infers that:

$$h \approx h_0 \tag{9}$$

with h_0, the h value for $t = 0$. On the other hand, one can assumed that h is directly connected to the deposit thickness d resulting from the electro-reduction of the metallic ions of the bath according to the Faraday law:

$$d = \frac{M\,q}{z\,F\rho}, \tag{10}$$

M, ρ, F and z keeping the same significance than in Section 2 while q represents the charge density. If one admits that the main part of the deposit is the one of the surface corrugations, it could be considered as having a low density and a thickness value of the same magnitude order than h, that is expressed as:

$$d \approx h. \tag{11}$$

For taking into account the two aspects, Alonso *et al.* [21,24] included a factor 2/3 to equation (7) that becomes:

$$\sigma = \frac{\pi\,h}{3\,r}\,. \tag{12}$$

A combination of equations (7, 9, 10) and (12) leads to a new expression of the surface roughness:

$$\sigma = \frac{\pi\,M\,q}{3\left(\dfrac{2\gamma\,a^4 D_\mathrm{s}}{\varepsilon_\mathrm{T}}\right)^{1/4}(z\,F\rho)t^{1/4}}\,. \tag{13}$$

This equation can be re-written to furthermore evidence the relationship between σ and t such as:

$$\frac{1}{\sigma} = \left[3\left(\frac{2\gamma\,a^4 D_\mathrm{s}}{\varepsilon_\mathrm{T}}\right)^{1/4}\left(\frac{z\,F\rho}{\pi\,M\,q}\right)\right]t^{1/4}. \tag{14}$$

The plotting of $1/\sigma$ *versus* $t^{1/4}$ in the time interval compatible with equation (7) leads to a straightline curve whose slope:

$$B = 3\left(\frac{2\gamma\,a^4 D_\mathrm{s}}{\varepsilon_\mathrm{T}}\right)^{1/4}\left(\frac{z\,\rho\,F}{\pi\,M\,q}\right) \tag{15}$$

allows the extraction of D_s, that is expressed as:

$$D_\mathrm{s} = \frac{\varepsilon_\mathrm{T}}{2\gamma\,a^4}\left(\frac{B\pi Mq}{3z\rho F}\right)^4. \tag{16}$$

This growth parameter gives a sight of the material surface formation that can be interpreted in term of relaxation which affects the universality class of the related interface.

As it appears, this model is based on the dynamics of the surface growth where the structure size or σ varies with the ageing time that is assimilated here to the material deposition duration. In this case, t is the only variable of the deposition process that is assumed to be directly proportional to d, v being constant. In the present work, the surface growth is investigated from alloy samples of the same thickness value. Therefore, t is inversely proportional to v that keeps the dependence of σ on t as above. Besides, the surface roughness used in this part is exclusively σ_sat since it is typical of the entire sample surface. The experimental variation of v and therefore that of t leading in Figure 4 to an increase and a decrease of σ_sat, the appropriate form of equation (14) to be considered here is:

$$\left|\frac{1}{\sigma_\mathrm{sat}}\right| = \left[3\left(\frac{2\gamma\,a^4 D_\mathrm{s}}{\varepsilon_\mathrm{T}}\right)^{1/4}\left(\frac{z\,F\rho}{\pi\,M\,q}\right)\right]t^{1/4}. \tag{14'}$$

5 Discussion

As expected, the results depict the dependence of the Ni-Zn composition on the range of the v values. Consequently, the evolution of the surface roughness as obtained can be ascribed to the alloy Ni content, as reported elsewhere [18]. The three linear regions of the $\sigma_\mathrm{sat} = f(v)$ curve in Figure 3 presumably correspond to different growth modes. Region 1, related to $v < 0.17$ μm/s, exhibits an increasing behaviour; region 2 located between 0.17 and 3.5 μm/s denotes a decreasing movement whilst a new increasing profile is obtained in region 3, over 3.5 μm/s. Each of the three regions are examined in the present section through the model proposed above considering the film formation in the large scale and also locally.

5.1 Change in the growth mode of the Ni-Zn alloy electrodeposits

The experimental data of Section 3 allow the plotting of the $|1/\sigma_\mathrm{sat}| = f(t^{1/4})$ for each of the three regions obtained with the σ_sat *versus* v curve. Figure 6 shows the related resulting linear trends that leads to the B values summarised in Table 4. $B = 2.41$ and 2.52 are obtained for regions 1 and 2 whilst the value 8.25 is relative to region 3. D_s is determined in accordance with equation (16) using the alloy physical parameters. $M = 62.04$ g/mole and $\rho = 8.02$ g/cm^3 are retained according to the evaluation proposed in Section 2. The common number of electrons transferred per mole of the concerned species is $z = 2$ with $q = 0.05$ C/cm^2, the charge density obtained in every case. The interface free energy $\gamma = 1320$ erg/cm^2 is averaged from those of the two elements (Ni and Zn) [26]. In view of the change in the alloy composition as shown in Figure 1, various structural phases are expected. For that reason, we take the average lattice parameter $a = 8.91 \times 10^{-8}$ cm [6]. Since the deposition is performed at $T = 323$ K, the related thermal energy is $\varepsilon_\mathrm{T} = 4.42 \times 10^{-14}$ erg.

The D_s values in Table 4, ranged between 10^{-10} and 3×10^{-8} cm^2/s, leads to the surface mobility of the adatoms in accordance with the Einstein relation. In our knowledge, no value from the literature is supplied regarding the growth of Ni-Zn alloy. One knows that Au and Pt electrodeposits prepared at the same temperature ($T = 323$ K) respectively led to 1.50×10^{-13} and 1.4×10^{-16} cm^2/s [24], that appear sensitively lower. The difference in the basic deposition conditions are certainly

Table 4. Surface diffusion coefficient (D_s) and diffusion length (Λ) of the ad-atoms in the formation of the Ni-Zn alloy electrodeposits.

Linear regions	v (μm/s)	t (s)	B	D_s (cm^2/s)	Λ (μm)
Region 1	$v < 0.17$	$25 < t < 62$	2.41	1.76×10^{-10}	0.85
Region 2	$0.17 < v < 0.35$	$7 < t < 12$	2.52	2.10×10^{-10}	0.45
Region 3	$v > 0.35$	$4 < t < 5$	8.24	2.40×10^{-8}	3.47

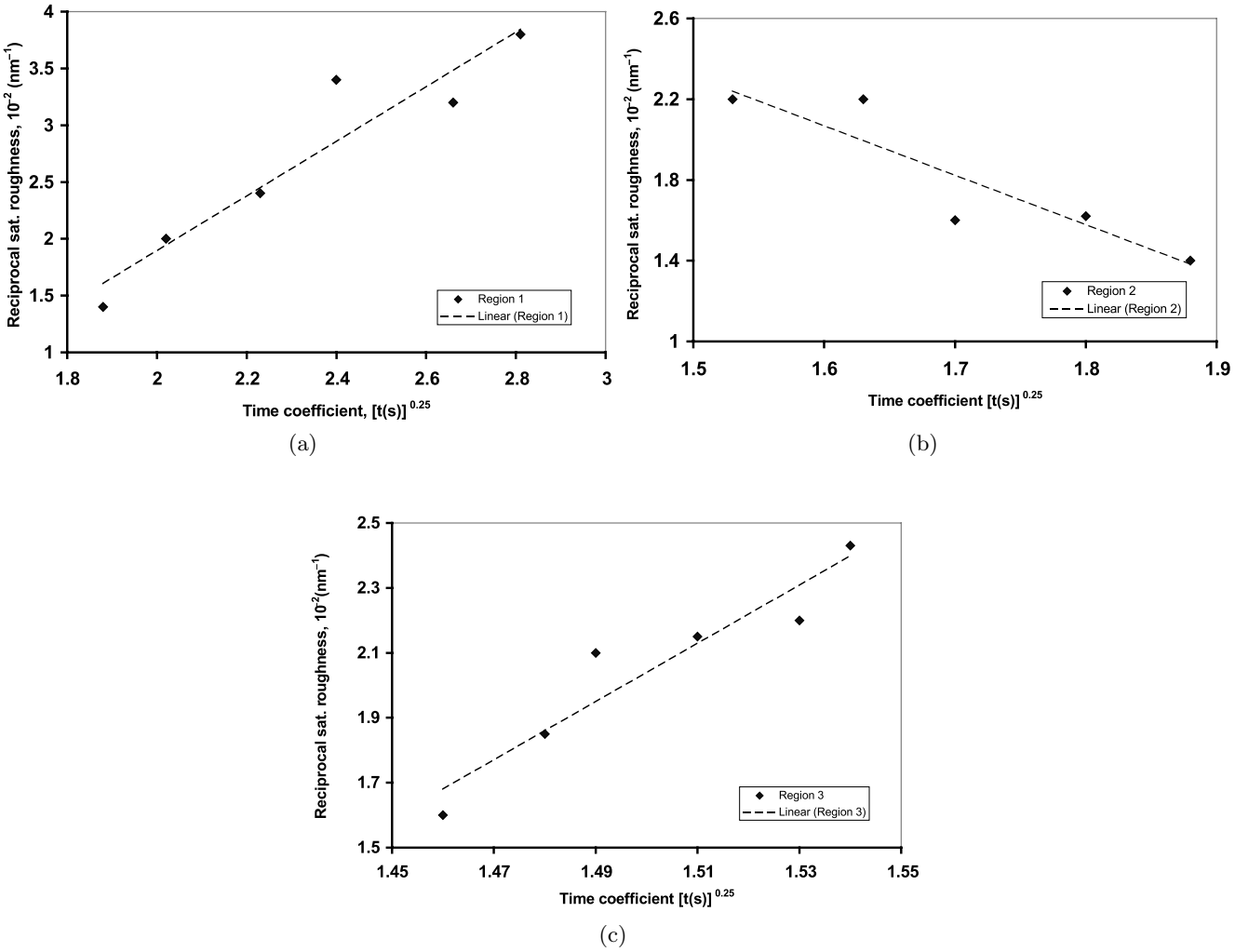

Fig. 6. Determination of the constant B for the study of the ad-atoms mobility as in the formation of the Ni-Zn alloy according to the regions of $\sigma_{sat} = f(v)$ curve in Figure 3: (a) for region 1; (b) for region 2; (c) for region 3.

for something. It should be mentioned that Au and Pt have both a markedly large atomic size compared to Ni and Zn. This size effect and the interfacial adsorption at the bath-substrate contact region [26] should be taken into account for the complete explanation of the D_s deviation. All these aspects together affect the re-crystallisation mechanisms and the resulting sample microstructure. Table 4 shows that the lower the v value, the smaller is D_s. However, the particle diffusion length, Λ, evaluated from the relation $\Lambda = (D_s t_m)^{1/2}$, with t_m the mean deposition time of the region, exhibits a decrease from $\Lambda = 0.85$ of region 1 to 0.45 μm of regions 2 before reaching the markedly increased value, 3.47 μm of region 3.

The results as obtained could be explained considering the relationship between the density of the nucleation sites n_s, linked to the substrate interface properties and the one of the ad-atoms formed, n_a, that is associated with v. A low v value implies a moderate flux of the cation species migrating towards the substrate, that engender a small n_a. The fulfilment of the condition $n_a \ll n_s$ implies

a relatively large mean free path of the ad-atoms before they stick at particular sites as a part of the substrate lattice. A large Λ value is expected in this case. An increase of v brings closer n_a to n_s, that reduces the mean free path of the ad-atoms, decreasing Λ value towards zero. This scenario satisfactorily explains the result $\Lambda = 0.85$ (region 1) $> \Lambda = 0.45$ μm/s (region 2) obtained here in agreement with the conclusion of Vazquez *et al.* [21]. The highest v values corresponding to $n_a \gg n_s$, means that there is a more intensive growing activity at the nucleation sites since the ad-atoms are supposed to be practically inert on the surface. This condition should favour the formation of conglomerated structures that also coalesce after reaching a critical size. This growth approach, exclusively based on the ad-atom quantity, remains unsatisfactory to explain the value $\Lambda = 3.47$ μm of region 3. It should be pointed out that no branched deposits suggesting a marked role of the non local phenomena is observed In Figure 4, this concurs with the commonly admitted effect of low v values [28]. Nevertheless, the morphological differences revealed by these AFM images infer that there are some changes in the material formation either in the initial stage (*i.e.* instantaneous or progressive nucleation) or in the next steps of the growth process. The columnar or needle-like structures of Figure 4a relative to region 1 have been explained to be a compromise between the Mullins-Sekerka instability effect which controls the column width and the impact of the local kinetics that leads to the lateral growth and surface roughness [28]. The top-rounded and more longitudinal structures of Figure 4d presuppose the predominance of the lateral growth in region 3, that implies a higher mobility of particles and therefore a larger Λ value, as here obtained. The two extreme microstructures of region 2 as shown in Figures 4b and c exhibit quite different grain size and shape certainly due to a relaxation phenomenon resulting in a morphological evolution that goes from the vertical pattern trend of region 1 to the horizontal one of region 3. The decrease of the σ_{sat} with the increase of v observed in region 2, as shown in Figure 3, is thereby explained.

5.2 Interface growth and the fractality of the Ni-Zn alloy surfaces

The existence of two linear portions below the saturation zone of the $\log \sigma = f(\log L)$ curves in Figure 5 has been already observed with the binary alloys of transition elements [18]. Besides, mono-atomic metal films such as silver [29], copper [30] and gold [31,32] obtained by various deposition methods also behave similarly. Many authors experimentally show that the mean size of the surface structures, $\langle d_s \rangle$, is nearly equal either to L_c for a single linear sloped portion of the curve or to L_0 when there is a double linear scaling feature. This relationship remains somewhat confusing in the second case since L_0 and L_c both coexist. Note that different regimes may develop in the same growth process, that are denoted by various shapes and sizes of the structures. Consequently, one can admit the presence of two distinguished structure types in the same surface whose mean size respectively corresponds to L_0 and L_c. Probably, only the largest structures (*i.e.* conglomerated ones) relative to one regime is measured as equivalent to L_c. Another regime associated with the smallest grains constituting the conglomerates appears in this case as related to L_0. This single or double structure features should be more easily analysed from the AFM top

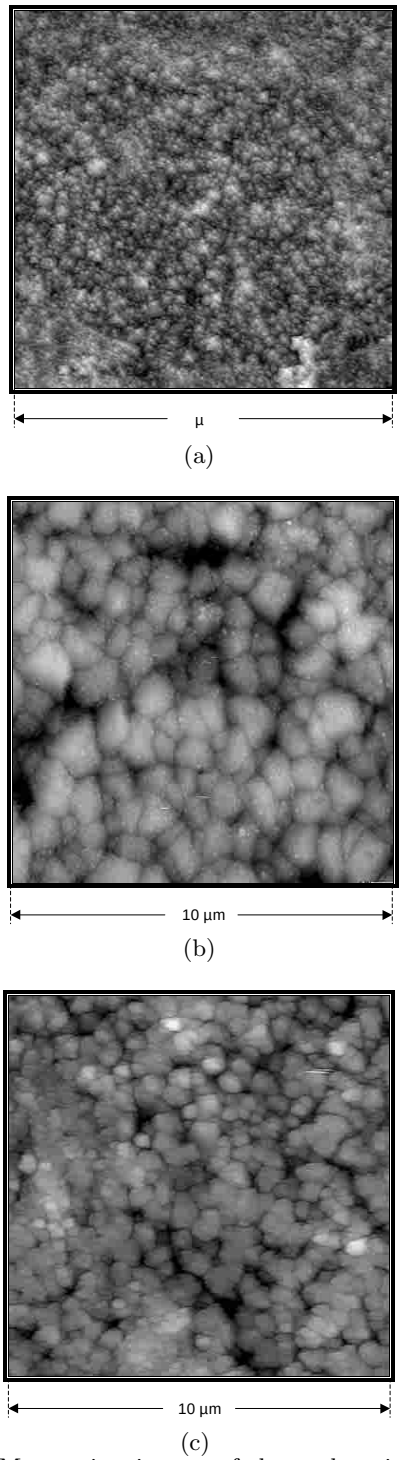

Fig. 7. AFM top view images of the as-deposited Ni-Zn alloy surfaces varying the growth velocity: (a) $v = 0.04$ μm/s; (b) $v = 0.16$ μm/s; (c) $v = 0.44$ μm/s.

view images of the sample surfaces. Unfortunately, this is not always visually distinguishable, particularly, when the grains of the second regime are markedly small. Their size difference denoted by ΔL in Table 2 is better expressed by the ratio L_c/L_0 which always remains close to 5. The large-scaled top view images of Figure 7 ($L = 10$ μm) show that the $\langle d_s \rangle$ value in each of the selected three images follow the behaviour of L_c *versus* v as proposed in Table 2. Besides, they clearly indicate the conglomeration trend of the structures for $v < 0.10$ μm/s (Fig. 7a) and $v > 0.30$ μm/s (Fig. 7c), that seems less noticeable for $v = 0.16$ μm/s as shown in Figure 7b.

Owing to the evolution of the Hurst exponent reported in Table 3, the surface microstructure of the Ni-Zn specimens results from different interface growth modes that can be here partially characterised. All of the exponent values are less than the unity, fulfilling the condition $0 < \alpha \leq 1$ required for a self-affine fractal surface texture [33], that appears here the common feature of our samples. Moreover, despite the splitting of the curve linearity observed in Figure 5 from $v = 0.10$ μm/s onwards, only one interface growth mode inherent to α value prevails. It should be mentioned that $0.60 \leq \alpha \leq 1$ as obtained here concurs with the roughness exponent reported for the ballistic or Eden deposition models described by the Kardar, Parizi and Zhang (KPZ) stochastic equation, including restricted surface diffusion for the three-dimensional Euclidean space [34–38]. Of course, the temporal scaling analysis leading to the determination of the growth and the dynamic exponents are required for deciding on the mode involved. In the assumption here of the KPZ dynamics, the result is likely to be a specific effect of the copper substrate which evidences the role of v in agreement with the data of Table 4. In actual fact, $\alpha = 0.60$ relative to $v < 0.10$ μm/s, is the smallest exponent obtained, the nearest one to 0.40 that is known as typical of the KPZ growth mode without restricted relaxation. This suggests that the mobility of the ad-atoms $\Lambda = 0.85$ μm reported for this v region is relatively limited. The large deviation of α from 0.40 till the mean value 0.81 inherent to the region $v > 0.35$ μm/s implies a more marked surface relaxation that is consistent with the increase of the ad-atom mobility till $\Lambda = 3.47$ μm in this region. Moreover, the irregular evolution of α for v ranged between 0.10 and 0.28 μm/s is corroborated by the particular behaviour of Λ values in the same v region. Probably, one deals in this region with a transitory topography due to the material compositional evolution as depicted in Figures 1 and 2 which directly affects the surface texture.

6 Conclusion

The reported work, based on the spatial behaviour of σ, can also be undertaken following the evolution of some other topography parameters describing the surface irregularities such as the average terrace width, η and the local slope, κ, for instance [39]. We point out that all of them are intimately related each other and η appears the more representative of the material active surface so important for the applied research on Ni-Zn thin films. Surface analyses by diffraction techniques providing a diffraction structure factor from which they can be directly extracted [40] are somewhat expensive methods. Real space techniques as SPM also lead to the determination of these parameters with the advantage of reaching the highest spatial resolutions. For that reason, the present study can be considered as only a preliminary step in this direction. In our objective of following the topological change of Ni-Zn electrodeposits induced by the lowest growth velocities, we show that the formation of this alloy films exclusively occurs here as an abnormal co-deposition phenomenon which is differently executed below 0.10 μm/s and beyond 0.20 μm/s. The evolution of the ratio (Ni_{al}/Ni_{sol}) *versus* v in each of these regions follows an hyperbolic law bearing specific coefficients. This behaviour is similar to the one previously observed for higher v values. Both, the morphology and the interface growth examined here through the behaviour of the surface roughness are affected by v value. The study of this growth process shows that the transport properties of the ad-atoms involved in the film formation vary. In every case, the alloy surfaces exhibit a roughness exponent in agreement with the dynamic growth mode of the KPZ analytical description including the restricted surface diffusion. However, the amplitude of this surface diffusion increases with the increase of v value.

References

1. N.R. Short, A. Abibsi, J.K. Dennis, Trans. Inst. Metal Finish **67**, 73 (1989).
2. A. Abibsi, N.R. Short, J.K. Dennis, Trans. Inst. Metal Finish **69**, 45 (1991).
3. K. Lohrberg, P. Kohl, Electrochim. Acta **29**, 2557 (1984).
4. E. Endoh, H. Otouma, T. Morimoto, Y. Oda, Int. J. Hydrogen Energy **12**, 473 (1987).
5. R. Fratesi, G. Roventi, G. Giuliani, C.R. Tomachuk, J. Appl. Electrochem. **27**, 1088 (1997).
6. L. Felloni, R. Fratesi, E. Quadrini, G. Roventi, J. Appl. Electrochem. **17**, 574 (1987).
7. F.J. Miranda, O.E. Barcia, O.R. Mattos, R. Wiart, J. Electrochem. Soc. **144**, 3441 (1997).
8. R. Albalat, E. Gòmez, C. Müller, M. Sarret, E. Vallès, J. Pregonas, J. Appl. Electrochem. **20**, 635 (1990).
9. C. Karwas, T. Hepel, J. Electrochem. Soc. **135**, 839 (1988).
10. M. Sikkens, I.J. Hodgkinson, F. Horowitz, H.A. Macleod, J. Wharton, Opt. Eng. **25**, 142 (1986).
11. J. Krim, I. Heyvaert, C. Van Haesendonck, Y. Bruynseraede, Phys. Rev. Lett. **70**, 57 (1993).
12. F. Family, Physica A **168**, 561 (1990).
13. J. Amar, F. Family, Phys. Rev. Lett. **64**, 543 (1990).
14. L.M. Sander, *The Physics of Structure Formation*, edited by W. Guttinger, G. Dangelmayr (Springer, London, 1987), p. 257.
15. D. Grier, E. Ben-Jacob, R. Clarke, L.M. Sander, Phys. Rev. Lett. **56**, 1264 (1986).
16. T.A. Witten, Jr, L.M. Sander, Phys. Rev. Lett. **47**, 1400 (1981).

17. P. Meakin, Phys. Rep. **235**, 189 (1993).
18. J. Ebothé, S. Vilain, J. Phys. D **32**, 2342 (1999).
19. A. Brenner, *Electrodeposition of alloys*, Vols. I and II (Academic Press, New York and London, 1963).
20. F. Family, J. Phys. A **19**, L441 (1986).
21. L. Vàsquez, A. Bartolome, A.M. Baro, C. Alonso, R.C. Salarezza, A.J. Arvia, Surf. Sci. **215**, 171 (1989).
22. M. Zinke-Allmang, L.C. Feldman, Appl. Surf. Sci. **52**, 357 (1991).
23. L.C. Feldman, M. Zinke-Allmang, J. Vac. Sci. Technol. A **8**, 3033 (1990).
24. C. Alonso, R.C. Salvarezza, J.M. Vara, A.J. Arvia, L. Vàzquez, A. Bartolome, A.M. Baro, J. Electrochem. Soc. **137**, 2161 (1990).
25. K. Carneiro, C.P. Jensen, J.F. Jorgensen, J. Garnoes, Ann. CIRP **44**, 517 (1995).
26. R.A. Swalin, *Thermodynamics of Solids*, edited by J.E. Burke, B. Chalmes, J.A. Krumhansl (J. Wiley & Sons, New York, London, Sydney, Toronto, 1972).
27. D.J. Trevor, C.E.D. Chidsey, D.N. Loiacono, Phys. Rev. **62**, 929 (1989).
28. G.L.M.K.S. Kahanda, X. Zou, R. Farrel, P. Wong, Phys. Rev. Lett. **25**, 3741 (1992).
29. I. Otsuka, T. Iwasaki, J. Vac. Sci. Technol. B **14**, 1153 (1996).
30. M. Cerisier, K. Attenborough, J. Fransaer, C. Van Haesendonck, J.-P. Celis, J. Electrochem. Soc. **146**, 2156 (1999).
31. L. Vàsquez, R.C. Salvarezza, P. Herrasti, P. Ocòn, J.M. Var, A.J. Arvia, Appl. Surf. Sci. **70/71**, 413 (1993).
32. R.C. Salvarezza, L. Vàzquez, P. Herrasti, P. Ocòn, M. Vara, A.J. Arvia, Europhys. Lett. **20**, 727 (1992).
33. A.L. Barabàsi, H.E. Stanley, *Fractal Concept in surface growth* (Cambridge University Press, New York 1995).
34. J. Villain, J. Phys. I **1**, 19 (1992).
35. S. Das Sarma, Phys. Rev. Lett. **66**, 2348 (1991).
36. M. Siegert, M. Plischke, Phys. Rev. Lett. **73**, 1517 (1994).
37. S. Mendez, G. Andreasen, P. Schilardi, M. Figueroa, L. Vàzquez, R.S. Salvarezza, A.J. Arvia, Langmir **14**, 2515 (1998).
38. R. Jullien, P. Meakin, Europhys. Lett. **4**, 1385 (1987).
39. H.-N. Yang, G.-C. Wang, T.-M. Lu, *Diffraction from Rough Surfaces and Dynamic Growth Fronts* (World Scientific, Singapore 1993).
40. Q. Jiang, H.-N. Yang, G.-C. Wang, J. Vac. Sci. Technol. B **14**, 3180 (1996).